

Casimir force for magnetodielectric media

Iver Brevik,^{1,*} Prachi Parashar,^{2,1,†} and K. V. Shajesh^{3,1,‡}

¹*Department of Energy and Process Engineering,
Norwegian University of Science and Technology, NO-7491 Trondheim, Norway*

²*John A. Logan College, Carterville, Illinois 62918, USA*

³*Department of Physics, Southern Illinois University–Carbondale, Carbondale, Illinois 62901, USA*
(Dated: October 4, 2018)

Boyer showed that a perfect electrically conducting slab repels a perfect magnetically conducting slab, in contrast to the attractive Casimir force between two identical perfect electrically or magnetically conducting slabs. To gain insight for the difference between the Boyer force and the Casimir force, we present the derivation of the Boyer force using the stress tensor method and then using the method of variation in dielectric. The Green dyadic, in terms of electric and magnetic Green's functions, is presented for an electric medium filling half of space and another magnetic medium filling another half of space such that the two half-spaces are parallel and separated by a distance a . We make the observation that the spectral distribution of scattering in a Boyer cavity is that of Fermi-Dirac type, while the spectral distribution of scattering in a Casimir cavity is that of Bose-Einstein type. Based on this observation we conclude that the difference between the Boyer force and the Casimir force is governed by the statistics of the possible scattering in the respective cavities.

I. INTRODUCTION

Consider the Boyer configuration of parallel slabs, consisting of two parallel semi-infinitely thick plates, separated by a vacuum gap a . Let the left plate be situated at $z = a_1$, the right plate at $z = a_2$, so that $a = a_2 - a_1$, see Fig. 1. Let the right plate be purely paramagnetic ($\mu > 1, \varepsilon = 1$), and the left plate purely dielectric ($\varepsilon > 1, \mu = 1$). The Boyer configuration of slabs should be contrasted with the Casimir configuration of parallel slabs in Fig. 2. We shall be interested in the pressure, called P here, between the slabs. For simplicity we limit ourselves to zero temperature. (General treatises on the Casimir effect can be found in Refs. [1–3].)

Stimulated by a suggestion from Casimir, Boyer [4] made an explicit calculation of the force between an infinitely permeable magnetic medium ($\mu \rightarrow \infty$) and a perfect conductor ($\varepsilon \rightarrow \infty$). The interaction energy per unit area was found to be

$$U = \frac{7}{8} \frac{\pi^2 \hbar c}{720 a^3}, \quad (1.1)$$

which corresponds to a *repulsive* pressure

$$P = \frac{7}{8} |P_0|, \quad (1.2)$$

where

$$P_0 = -\frac{\pi^2 \hbar c}{240 a^4} \quad (1.3)$$

is the attractive force between two perfectly conducting plates. As explained by Boyer, this is related to the fact that while an electrically polarizable particle is attracted to a conducting wall, a magnetically polarizable particle is repelled by it (the latter case being analogous to the hydrodynamic flow from a point or line source outside an impenetrable plane).

From the standpoint of optical physics this result is however rather perplexing. Consider for definiteness the electromagnetic force density \mathbf{f} on the boundary layer in the left plate; this force is purely electric, and is calculated from the divergence of Maxwell's stress tensor to be

$$\mathbf{f} = -\frac{1}{2} E^2 \nabla \varepsilon. \quad (1.4)$$

In classical physics this force always acts towards the optically thinner medium, that is, towards the vacuum region for the plate in consideration. One can observe that the *direction* of this force given by the direction of $\nabla \varepsilon$ is independent of the magnetic properties of the right plate. The direction is determined by the gradient of the dielectric permittivity ε only. Even if the magnetic properties of the right plate should change, the electric field \mathbf{E} on the left plate would change, but the direction of this force would be just the same.

The magnitude of the surface pressure P can be found by integrating the normal component f_z across the boundary located at $z = a_1$. Now there are numerous cases in optics showing the reality of the expression in Eq. (1.4). For example, the classic experiment of Ashkin and Dziedzic [5], demonstrating the outward bulge of a water surface illuminated by a radiation beam coming from above, is of this sort, as is the newer version of this experiment due to Astrath et al. [6] (a review of some radiation pressure experiments of this sort can be found in Ref. [7]). Also, the recent pressure experiment of Kundu et al. [8], showing the deflection of a graphene sheet upon

* iver.h.brevik@ntnu.no

† Prachi.Parashar@jalc.edu

‡ kvshajesh@gmail.com

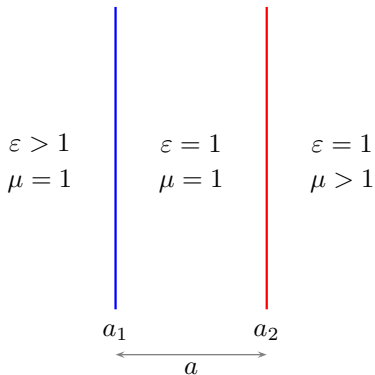


FIG. 1. Boyer configuration of parallel slabs.

laser illumination, belongs to the same category. In all these cases, the force was found to act in the direction of the optically thinner medium, in accordance with the expression in Eq. (1.4).

If one leaves the regime of classical physics and moves on to the quantum mechanical calculation of the Casimir pressure, one finds analogous results as long as both plates, separated by a vacuum gap, are either *purely dielectric or purely magnetic*. This pressure is conventionally calculated by taking the difference between the zz components of Maxwell's stress tensor on the two sides, making use of the fluctuation-dissipation theorem when constructing the two-point functions for the electric and magnetic fields. Again, the pressure is found to be attractive, in accordance with Eq. (1.4).

Now return to the magnetodielectric case considered by Boyer. At first glance one would think that the repulsiveness of the force as mentioned above is in direct conflict with Eq. (1.4). What is the physical reason for this? Formally, the situation would mean that one has to reverse the sign of the quadratic quantity E^2 in Eq. (1.4). In view of this bizarre situation, one would think that a revisit of the fundamental assumptions behind electromagnetic theory in matter is desirable. That was one of the motivations behind the present paper.

We first present the Green function formalism in a general way in Sec. II, and provide explicit solutions for the Green dyadic in Sec. III, where the two plates are each allowed to possess arbitrary, even frequency-dependent, values of μ and ε , and calculate the surface force formally in Sec. IV. Thereafter we specialize to the Boyer case. We make the observation that the spectral distribution of scattering in a Boyer cavity is that of Fermi-Dirac type, while the spectral distribution of scattering in a Casimir cavity is that of Bose-Einstein type. Based on this observation we suggest that the difference between the Boyer force and the Casimir force is statistics of the possible scattering in the respective cavities.

Next, we inquire if the Boyer force is sensitive to a cutoff in the frequency response of permeability μ . Cal-

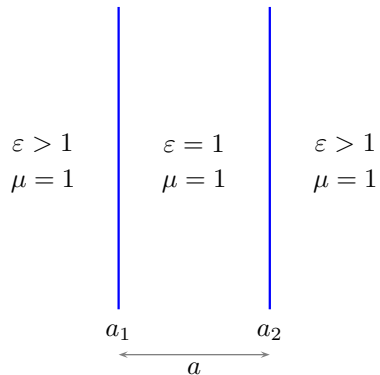


FIG. 2. Casimir configuration of parallel slabs.

culations of the Boyer force have usually assumed μ to be a constant for all frequencies. It is easy to see that this is a over-simplified model that violates one of the fundamentals of macroscopic theory (cf. also the discussion in Ref. [9]): Start from the “microscopic” Maxwell equation (here in Heaviside-Lorentz units)

$$\nabla \times \mathbf{h} = \rho \mathbf{v} + \frac{\partial \mathbf{e}}{\partial t}, \quad (1.5)$$

where $\rho \mathbf{v}$ is the local current density and \mathbf{h} and \mathbf{e} are the local magnetic and electric fields. Space averaging gives $\bar{\mathbf{h}} = \mathbf{B}$ with \mathbf{B} the magnetic induction, and $\bar{\mathbf{e}} = \mathbf{E}$ with \mathbf{E} the macroscopic electric field. Thus

$$\nabla \times \mathbf{B} = \bar{\rho} \mathbf{v} + \frac{\partial \mathbf{E}}{\partial t}. \quad (1.6)$$

Subtracting the Maxwell equation $\nabla \times \mathbf{H} = \partial \mathbf{D} / \partial t$ we get

$$\bar{\rho} \mathbf{v} = \nabla \times \mathbf{M} + \frac{\partial \mathbf{P}}{\partial t}, \quad (1.7)$$

with $\mathbf{M} = \mathbf{B} - \mathbf{H}$ and $\mathbf{P} = \mathbf{D} - \mathbf{E}$.

Consider now the general definition of the magnetic moment \mathbf{m} of a body,

$$\mathbf{m} = \frac{1}{2} \int \mathbf{r} \times \bar{\rho} \mathbf{v} dV. \quad (1.8)$$

This can be compared with the expression

$$\frac{1}{2} \int \mathbf{r} \times (\nabla \times \mathbf{M}) dV = \int \mathbf{M} dV, \quad (1.9)$$

which is derived using vector manipulations observing that $\mathbf{M} = 0$ in the vacuum region outside the body. Since $\mathbf{m} = \int \mathbf{M} dV$ it follows that we can put $\bar{\rho} \mathbf{v}$ equal to $\nabla \times \mathbf{M}$. Comparing with Eq. (1.7) we conclude that the consistency of macroscopic electrodynamics depends on the possibility to neglect the $\partial \mathbf{P} / \partial t$ term. This can be made concrete further by assuming that the body of

linear size l is exposed to an electromagnetic wave of frequency ω . We shall insert speed of light c , momentarily, in expressions in this section for the benefit of the reader. Order of magnitude estimates give $\partial P/\partial t \sim \omega E \sim \omega^2 l H/c$ (the relationship $E \sim \omega l H/c$ used in the last estimate coming from the equation $\nabla \times \mathbf{E} = -\partial \mathbf{B}/\partial t$ and $E \sim H$). The first term on the right hand side of Eq. (1.7) is $\nabla \times \mathbf{M} = \chi \nabla \times \mathbf{H}$ where χ is the susceptibility, and is estimated to be of order $c\chi H/l$. Thus, our consistency condition reduces to

$$l^2 \ll \chi c^2 / \omega^2; \quad (1.10)$$

an inequality already given in Ref. [9]. It is easily seen that the inequality in Eq. (1.10) is broken already at frequencies ω much less than optical frequencies. And that is confirmed by experiments also. For instance, for ferrite with $\mu \approx 600$ the maximum of the frequency $\omega/2\pi$ is reported to lie in the region 100 kHz to 1 MHz [10]. The assumption about a very large and constant permeability as used in the Boyer calculation is obviously unphysical.

In Sec. V we take the magnetic dispersion into account in a crude way, by assuming μ to be constant up to a critical value $\omega = \omega_c$. For higher frequencies we set $\mu = 1$. Thus

$$\mu(\omega) = \begin{cases} \mu, & \omega < \omega_c, \\ 1, & \omega > \omega_c. \end{cases} \quad (1.11)$$

As one might expect, we do not find a reversal of the sign of the force in this way; the force still comes out repulsive. So the basic problem alluded to at the beginning, is not solved. However, an important physical result of the calculation is that the force turns out to be immeasurably small, when realistic input data for ω_c are inserted. This makes it evident why the repulsive force has never been measured. It may finally be mentioned that we will keep ε constant, at all frequencies. There is no comparably strong limit to the permittivity as it is to the permeability.

In Sec. VI we consider the Boyer problem from a statistical mechanical point of view, introducing a model where the two media are represented by harmonic oscillators 1 and 2, interacting with each other via a third oscillator 3. In this way a mechanical analogue to the conventional TE and TM modes in electromagnetism is obtained. We find that the quantum mechanical transition from the TM to the TE mode, implying that oscillator 3 interacts with oscillators 1 and 2 via canonical momenta instead of positions, is an important point. In this way the statistical mechanical analysis helps us to elucidate the problem.

II. MAXWELL'S EQUATIONS

In Heaviside-Lorentz units the monochromatic components of Maxwell's equations, proportional to $\exp(-i\omega t)$, in the absence of net charges and currents, and in pres-

ence of dielectric and magnetic materials with boundaries, are

$$\nabla \times \mathbf{E} = i\omega \mathbf{B}, \quad (2.1a)$$

$$-\nabla \times \mathbf{H} = i\omega(\mathbf{D} + \mathbf{P}). \quad (2.1b)$$

These equations imply $\nabla \cdot \mathbf{B} = 0$ and $\nabla \cdot (\mathbf{D} + \mathbf{P}) = 0$. Here \mathbf{P} is an external source of polarization, in addition to the polarization of the material in response to the fields \mathbf{E} and \mathbf{H} . The external source \mathbf{P} serves as a convenient mathematical tool, and is set to zero in the end. In the following we neglect non-linear responses and assume that the fields \mathbf{D} and \mathbf{B} respond linearly to the electric and magnetic fields \mathbf{E} and \mathbf{H} :

$$\mathbf{D}(\mathbf{r}, \omega) = \varepsilon(\mathbf{r}; \omega) \cdot \mathbf{E}(\mathbf{r}, \omega), \quad (2.2a)$$

$$\mathbf{B}(\mathbf{r}, \omega) = \mu(\mathbf{r}; \omega) \cdot \mathbf{H}(\mathbf{r}, \omega). \quad (2.2b)$$

Using Eq. (2.1a) in Eq. (2.1b) we construct the following differential equation for the electric field,

$$\left[\frac{1}{\omega^2} \nabla \times \mu^{-1} \cdot \nabla \times -1 - \chi \right] \cdot \mathbf{E}(\mathbf{r}, \omega) = \mathbf{P}(\mathbf{r}, \omega), \quad (2.3)$$

where

$$\chi(\mathbf{r}; \omega) = \varepsilon(\mathbf{r}; \omega) - 1. \quad (2.4)$$

The differential equation for the Green's dyadic $\Gamma(\mathbf{r}, \mathbf{r}'; \omega)$ is guided by Eq. (2.3),

$$\left[\frac{1}{\omega^2} \nabla \times \mu^{-1} \cdot \nabla \times -1 - \chi \right] \cdot \Gamma(\mathbf{r}, \mathbf{r}'; \omega) = \mathbf{1} \delta^{(3)}(\mathbf{r} - \mathbf{r}'). \quad (2.5)$$

It defines the relation between the electric field and the polarization source,

$$\mathbf{E}(\mathbf{r}; \omega) = \int d^3 r' \Gamma(\mathbf{r}, \mathbf{r}'; \omega) \cdot \mathbf{P}(\mathbf{r}'; \omega). \quad (2.6)$$

The corresponding dyadic for vacuum, obtained by setting $\chi = 0$, is called the free Green's dyadic and satisfies the equation

$$\left[\frac{1}{\omega^2} \nabla \times \mu^{-1} \cdot \nabla \times -1 \right] \cdot \Gamma_0(\mathbf{r}, \mathbf{r}'; \omega) = \mathbf{1} \delta^{(3)}(\mathbf{r} - \mathbf{r}'). \quad (2.7)$$

We can also define the relation between the magnetic field and the polarization source,

$$\mathbf{H}(\mathbf{r}; \omega) = \int d^3 r' \Phi(\mathbf{r}, \mathbf{r}'; \omega) \cdot \mathbf{P}(\mathbf{r}'; \omega). \quad (2.8)$$

A. Quantum electrodynamics

The Green dyadics gives the correlation between the fields and sources, as per Eqs. (2.6) and (2.8),

$$\frac{\delta \mathbf{E}(\mathbf{r}; \omega)}{\delta \mathbf{P}(\mathbf{r}'; \omega)} = \Gamma(\mathbf{r}, \mathbf{r}'; \omega), \quad (2.9a)$$

$$\frac{\delta \mathbf{H}(\mathbf{r}; \omega)}{\delta \mathbf{P}(\mathbf{r}'; \omega)} = \Phi(\mathbf{r}, \mathbf{r}'; \omega). \quad (2.9b)$$

In quantum electrodynamics the Green dyadics also serve as correlations between the fields at two different points in space, which are stated as

$$\frac{1}{\tau} \langle \mathbf{E}(\mathbf{r}; -\omega) \mathbf{E}(\mathbf{r}'; \omega) \rangle = \frac{1}{i} \mathbf{\Gamma}(\mathbf{r}, \mathbf{r}'; \omega), \quad (2.10a)$$

$$\frac{1}{\tau} \langle \mathbf{H}(\mathbf{r}; -\omega) \mathbf{H}(\mathbf{r}'; \omega) \rangle = \frac{1}{i} \mathbf{\Gamma}(\mathbf{r}, \mathbf{r}'; \omega) \Big|_{E \leftrightarrow H, \varepsilon \leftrightarrow \mu}, \quad (2.10b)$$

$$\frac{1}{\tau} \langle \mathbf{H}(\mathbf{r}; -\omega) \mathbf{E}(\mathbf{r}'; \omega) \rangle = \frac{1}{i} \mathbf{\Phi}(\mathbf{r}, \mathbf{r}'; \omega) \quad (2.10c)$$

$$\frac{1}{\tau} \langle \mathbf{E}(\mathbf{r}; -\omega) \mathbf{H}(\mathbf{r}'; \omega) \rangle^* = \frac{1}{i} \mathbf{\Phi}(\mathbf{r}, \mathbf{r}'; \omega), \quad (2.10d)$$

where τ is the average (infinite) time for which the system is observed.

III. GREEN'S DYADIC

For planar geometry, using translational symmetry in the plane, we can define the Fourier transformations

$$\mathbf{\Gamma}(\mathbf{r}, \mathbf{r}'; \omega) = \int \frac{d^2 k_{\perp}}{(2\pi)^2} e^{i\mathbf{k}_{\perp} \cdot (\mathbf{r} - \mathbf{r}')_{\perp}} \boldsymbol{\gamma}(z, z'; k_{\perp}, \omega), \quad (3.1a)$$

$$\mathbf{\Phi}(\mathbf{r}, \mathbf{r}'; \omega) = \int \frac{d^2 k_{\perp}}{(2\pi)^2} e^{i\mathbf{k}_{\perp} \cdot (\mathbf{r} - \mathbf{r}')_{\perp}} \boldsymbol{\phi}(z, z'; k_{\perp}, \omega). \quad (3.1b)$$

The reduced Green's dyadics can be expressed in the form

$$\boldsymbol{\gamma} = \begin{bmatrix} \frac{1}{\varepsilon^{\perp}(z)} \frac{\partial}{\partial z} \frac{1}{\varepsilon^{\perp}(z')} \frac{\partial}{\partial z'} g^H & 0 & \frac{1}{\varepsilon^{\perp}(z)} \frac{\partial}{\partial z} \frac{ik_{\perp}}{\varepsilon^{\parallel}(z')} g^H \\ 0 & \omega^2 g^E & 0 \\ -\frac{ik_{\perp}}{\varepsilon^{\parallel}(z)} \frac{1}{\varepsilon^{\perp}(z')} \frac{\partial}{\partial z'} g^H & 0 & -\frac{ik_{\perp}}{\varepsilon^{\parallel}(z)} \frac{ik_{\perp}}{\varepsilon^{\parallel}(z')} g^H \end{bmatrix}. \quad (3.2)$$

Here we have omitted the term

$$-\delta(z - z') \begin{bmatrix} \frac{1}{\varepsilon^{\perp}(z)} & 0 & 0 \\ 0 & 0 & 0 \\ 0 & 0 & \frac{1}{\varepsilon^{\parallel}(z)} \end{bmatrix} \quad (3.3)$$

that contains a δ -function and thus never contributes to interaction energies between two bodies unless they are overlapping, and

$$\boldsymbol{\phi} = i\omega \begin{bmatrix} 0 & \frac{1}{\mu^{\perp}(z)} \frac{\partial}{\partial z} g^E & 0 \\ \frac{1}{\varepsilon^{\perp}(z')} \frac{\partial}{\partial z'} g^H & 0 & \frac{ik_{\perp}}{\varepsilon^{\parallel}(z')} g^H \\ 0 & -\frac{ik_{\perp}}{\mu^{\parallel}(z)} g^E & 0 \end{bmatrix}. \quad (3.4)$$

Here the magnetic (TM mode) Green's function $g^H(z, z')$, and the electric (TE mode) Green's function $g^E(z, z')$, are defined using the differential equations

$$\left[-\frac{\partial}{\partial z} \frac{1}{\varepsilon^{\perp}(z)} \frac{\partial}{\partial z} + \frac{k_{\perp}^2}{\varepsilon^{\parallel}(z)} - \omega^2 \mu^{\perp}(z) \right] g^H = \delta(z - z'), \quad (3.5a)$$

$$\left[-\frac{\partial}{\partial z} \frac{1}{\mu^{\perp}(z)} \frac{\partial}{\partial z} + \frac{k_{\perp}^2}{\mu^{\parallel}(z)} - \omega^2 \varepsilon^{\perp}(z) \right] g^E = \delta(z - z'), \quad (3.5b)$$

where $\varepsilon = \text{diag}(\varepsilon^{\perp}, \varepsilon^{\perp}, \varepsilon^{\parallel})$ is the permittivity tensor and $\mu = \text{diag}(\mu^{\perp}, \mu^{\perp}, \mu^{\parallel})$ is the permeability tensor [11].

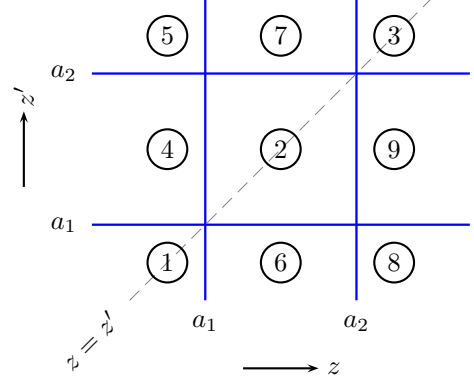


FIG. 3. Labels for the regions in the z - z' space, used for specifying the Green function.

A. Electric Green's function for Boyer configuration

For the Boyer configuration of slabs in Fig. 1 with isotropic permittivity ε and permeability μ we have the differential equation for the electric Green's function

$$\left[-\frac{\partial}{\partial z} \frac{1}{\mu(z)} \frac{\partial}{\partial z} + \frac{k_{\perp}^2}{\mu(z)} - \omega^2 \varepsilon(z) \right] g^E(z, z') = \delta(z - z'), \quad (3.6)$$

where

$$\varepsilon(z) = 1 + (\varepsilon - 1) \theta(a_1 - z), \quad (3.7a)$$

$$\mu(z) = 1 + (\mu - 1) \theta(z - a_2), \quad (3.7b)$$

with boundary conditions

$$g^E(z, z') \Big|_{a_i - \delta}^{a_i + \delta} = 0, \quad (3.8a)$$

$$\left\{ \frac{1}{\mu(z)} \frac{\partial}{\partial z} g^E(z, z') \right\} \Big|_{a_i - \delta}^{a_i + \delta} = 0. \quad (3.8b)$$

In terms of shorthand notations for typesetting

$$\kappa = \sqrt{k_{\perp}^2 + \zeta^2}, \quad (3.9)$$

and

$$\kappa_{\varepsilon} = \sqrt{k_{\perp}^2 + \zeta^2 \varepsilon}, \quad \kappa_{\mu} = \sqrt{k_{\perp}^2 + \zeta^2 \mu}, \quad (3.10)$$

and

$$\bar{\kappa}_{\varepsilon} = \frac{\kappa_{\varepsilon}}{\varepsilon}, \quad \bar{\kappa}_{\mu} = \frac{\kappa_{\mu}}{\mu}, \quad (3.11)$$

and

$$r_{\varepsilon} = r_1^E = \frac{\kappa_{\varepsilon} - \kappa}{\kappa_{\varepsilon} + \kappa}, \quad r_2^E = 0, \quad (3.12a)$$

$$r_1^H = 0, \quad r_2^H = \frac{\bar{\kappa}_{\mu} - \kappa}{\bar{\kappa}_{\mu} + \kappa} = r_{\mu}, \quad (3.12b)$$

and

$$\Delta^E = 1 - r_\varepsilon \bar{r}_\mu e^{-2\kappa a}, \quad (3.13a)$$

$$\Delta^H = 1 - \bar{r}_\varepsilon r_\mu e^{-2\kappa a}, \quad (3.13b)$$

where \bar{r}_ε is obtained by replacing $\kappa_\varepsilon \rightarrow \bar{\kappa}_\varepsilon$ in r_ε , and, similarly, \bar{r}_μ is obtained by replacing $\kappa_\mu \rightarrow \bar{\kappa}_\mu$ in r_μ .

In the following the label in the subscript represents the region in Fig. 3 in which the variables z and z' reside. The solution for the electric Green's function is,

$$g_{\textcircled{1}}^E(z, z') = \frac{1}{2\kappa_\varepsilon} e^{-\kappa_\varepsilon |z-z'|} + \frac{1}{2\kappa_\varepsilon} \frac{1}{\Delta^E} [r_\varepsilon - \bar{r}_\mu e^{-2\kappa a}] e^{-\kappa_\varepsilon |a_1-z|} e^{-\kappa_\varepsilon |a_1-z'|}, \quad z, z' < a_1 < a_2, \quad (3.14a)$$

$$g_{\textcircled{4}}^E(z, z') = \frac{1}{\kappa_\varepsilon + \kappa} \frac{1}{\Delta^E} e^{-\kappa_\varepsilon |a_1-z|} e^{-\kappa |z'-a_1|} - \frac{1}{\kappa_\varepsilon + \kappa} \frac{1}{\Delta^E} [\bar{r}_\mu e^{-\kappa a}] e^{-\kappa_\varepsilon |a_1-z|} e^{-\kappa |a_2-z'|}, \quad z < a_1 < z' < a_2, \quad (3.14b)$$

$$g_{\textcircled{5}}^E(z, z') = \frac{1}{2\kappa} \frac{1}{\Delta^E} \left[\frac{2\kappa}{\kappa_\varepsilon + \kappa} \frac{2\kappa}{\bar{\kappa}_\mu + \kappa} e^{-\kappa a} \right] e^{-\kappa_\varepsilon |a_1-z|} e^{-\kappa_\mu |z'-a_2|}, \quad z < a_1 < a_2 < z', \quad (3.14c)$$

and

$$g_{\textcircled{6}}^E(z, z') = \frac{1}{\kappa_\varepsilon + \kappa} \frac{1}{\Delta^E} e^{-\kappa |z-a_1|} e^{-\kappa_\varepsilon |a_1-z'|} - \frac{1}{\kappa_\varepsilon + \kappa} \frac{1}{\Delta^E} [\bar{r}_\mu e^{-\kappa a}] e^{-\kappa |a_2-z|} e^{-\kappa_\varepsilon |a_1-z'|}, \quad z' < a_1 < z < a_2, \quad (3.15a)$$

$$g_{\textcircled{2}}^E(z, z') = \frac{1}{2\kappa} e^{-\kappa |z-z'|} - \frac{1}{2\kappa} \frac{1}{\Delta^E} [r_\varepsilon] e^{-\kappa |z-a_1|} e^{-\kappa |z'-a_1|} + \frac{1}{2\kappa} \frac{1}{\Delta^E} [r_\varepsilon \bar{r}_\mu e^{-\kappa a}] e^{-\kappa |z-a_1|} e^{-\kappa |a_2-z'|} \\ + \frac{1}{2\kappa} \frac{1}{\Delta^E} [\bar{r}_\mu r_\varepsilon e^{-\kappa a}] e^{-\kappa |a_2-z|} e^{-\kappa |z'-a_1|} - \frac{1}{2\kappa} \frac{1}{\Delta^E} [\bar{r}_\mu] e^{-\kappa |a_2-z|} e^{-\kappa |a_2-z'|}, \quad a_1 < z', z < a_2, \quad (3.15b)$$

$$g_{\textcircled{7}}^E(z, z') = \frac{1}{\bar{\kappa}_\mu + \kappa} \frac{1}{\Delta^E} e^{-\kappa |a_2-z|} e^{-\kappa_\mu |z'-a_2|} - \frac{1}{\bar{\kappa}_\mu + \kappa} \frac{1}{\Delta^E} [r_\varepsilon e^{-\kappa a}] e^{-\kappa |z-a_1|} e^{-\kappa_\mu |z'-a_2|}, \quad a_1 < z < a_2 < z', \quad (3.15c)$$

and

$$g_{\textcircled{8}}^E(z, z') = \frac{1}{2\kappa} \frac{1}{\Delta^E} \left[\frac{2\kappa}{\kappa_\varepsilon + \kappa} \frac{2\kappa}{\bar{\kappa}_\mu + \kappa} e^{-\kappa a} \right] e^{-\kappa_\mu |z-a_2|} e^{-\kappa_\varepsilon |a_1-z'|}, \quad z' < a_1 < a_2 < z, \quad (3.16a)$$

$$g_{\textcircled{9}}^E(z, z') = \frac{1}{\bar{\kappa}_\mu + \kappa} \frac{1}{\Delta^E} e^{-\kappa_\mu |z-a_2|} e^{-\kappa |a_2-z'|} - \frac{1}{\bar{\kappa}_\mu + \kappa} \frac{1}{\Delta^E} [r_\varepsilon e^{-\kappa a}] e^{-\kappa_\mu |z-a_2|} e^{-\kappa |z'-a_1|}, \quad a_1 < z' < a_2 < z, \quad (3.16b)$$

$$g_{\textcircled{3}}^E(z, z') = \frac{1}{2\bar{\kappa}_\mu} e^{-\kappa_\mu |z-z'|} + \frac{1}{2\bar{\kappa}_\mu} \frac{1}{\Delta^E} [\bar{r}_\mu - r_\varepsilon e^{-2\kappa a}] e^{-\kappa_\mu |z-a_2|} e^{-\kappa_\mu |z'-a_2|}, \quad a_1 < a_2 < z', z. \quad (3.16c)$$

B. Magnetic Green's function for Boyer configuration

For the Boyer configuration of slabs in Fig. 3 the magnetic Green's function has the differential equation

$$\left[-\frac{\partial}{\partial z} \frac{1}{\varepsilon(z)} \frac{\partial}{\partial z} + \frac{k_1^2}{\varepsilon(z)} - \omega^2 \mu(z) \right] g^H(z, z') = \delta(z - z'), \quad (3.17)$$

with boundary conditions

$$g^H(z, z') \Big|_{a_i-\delta}^{a_i+\delta} = 0, \quad (3.18a)$$

$$\left\{ \frac{1}{\varepsilon(z)} \frac{\partial}{\partial z} g^H(z, z') \right\} \Big|_{a_i-\delta}^{a_i+\delta} = 0. \quad (3.18b)$$

The solution for the magnetic Green's function is obtained from the electric Green's function by replacing

$\kappa_\varepsilon \rightarrow \bar{\kappa}_\varepsilon$ and $\bar{\kappa}_\mu \rightarrow \kappa_\mu$ everywhere, except in the exponentials. This leads to the replacements, $r_\varepsilon \rightarrow \bar{r}_\varepsilon$, $\bar{r}_\mu \rightarrow r_\mu$, and $\Delta^E \rightarrow \Delta^H$.

C. Perfect electric and magnetic conductors

In the limit $\varepsilon \rightarrow \infty$ and $\mu \rightarrow \infty$, when the region $z < a_1$ is a perfectly conducting electric medium and the region $z > a_1$ is a perfectly conducting magnetic material, we observe that the region corresponding to $a_1 < z, z' < a_2$ in Fig. 1 is the only relevant region in the discussion as the fields vanish inside the two perfectly conducting media. Thus, we have

$$\Delta_{\text{PC}} = 1 + e^{-2\kappa a}. \quad (3.19)$$

In this case, the explicit form for the Green functions can be conveniently expressed as

$$g^E(z, z') = \frac{1}{\kappa} \frac{\sinh \kappa(z_{<} - a_1) \cosh \kappa(z_{>} - a_2)}{\cosh \kappa a}, \quad (3.20a)$$

$$g^H(z, z') = -\frac{1}{\kappa} \frac{\cosh \kappa(z_{<} - a_1) \sinh \kappa(z_{>} - a_2)}{\cosh \kappa a}, \quad (3.20b)$$

which is evaluated in region ②. Here $z_{<} = \text{Min}(z, z')$ and $z_{>} = \text{Max}(z, z')$. We make the observation that, on the boundaries of the perfectly conducting slabs at $z = a_1$ and $z = a_2$ of the Boyer configuration we have

$$g^E(a_1, a_2) = 0, \quad g^E(a_2, a_2) = \frac{\tanh \kappa a}{\kappa}, \quad (3.21a)$$

$$g^E(a_1, a_1) = 0, \quad g^E(a_2, a_1) = \frac{\sinh \kappa a}{\kappa}, \quad (3.21b)$$

and

$$g^H(a_1, a_2) = 0, \quad g^H(a_2, a_2) = 0, \quad (3.22a)$$

$$g^H(a_1, a_1) = \frac{\tanh \kappa a}{\kappa}, \quad g^H(a_2, a_1) = \frac{\sinh \kappa a}{\kappa}. \quad (3.22b)$$

We further make the observation that

$$\frac{\partial}{\partial z} \frac{\partial}{\partial z'} g^E(z, z') = -\kappa^2 g^H(z, z'), \quad (3.23a)$$

$$\frac{\partial}{\partial z} \frac{\partial}{\partial z'} g^H(z, z') = -\kappa^2 g^E(z, z'), \quad (3.23b)$$

such that

$$\begin{aligned} \frac{\partial}{\partial z} \frac{\partial}{\partial z'} \left[g^E(z, z') + g^H(z, z') \right] \Big|_{z=a_1, z'=a_1} \\ = -\kappa^2 \left[g^E(z, z') + g^H(z, z') \right], \end{aligned} \quad (3.24)$$

and

$$g^E(a_1, a_1) + g^H(a_1, a_1) = \frac{\tanh \kappa a}{\kappa}. \quad (3.25)$$

IV. STRONG COUPLING: BOYER'S RESULT

For slowly varying fields, and assuming that the dissipation in the system is negligible, the statement of conservation of momentum density,

$$\rho \mathbf{E} + \rho \mathbf{v} \times \mathbf{B} + \frac{\partial \mathbf{G}}{\partial t} + \nabla \cdot \mathbf{T} - \frac{1}{2} E^2 \nabla \varepsilon - \frac{1}{2} H^2 \nabla \mu = 0, \quad (4.1)$$

can be derived starting from the Maxwell equations [12], where

$$\mathbf{G} = \mathbf{D} \times \mathbf{B} \quad (4.2)$$

is the momentum density of the electromagnetic field and

$$\mathbf{T} = \mathbf{1} \frac{1}{2} (\mathbf{D} \cdot \mathbf{E} + \mathbf{B} \cdot \mathbf{H}) - (\mathbf{D}\mathbf{E} + \mathbf{B}\mathbf{H}) \quad (4.3)$$

is the stress tensor or the flux of the momentum density of the electromagnetic field. Each term in Eq. (4.1) is interpreted as a force when it is integrated over a volume V . The first two terms in Eq. (4.1), together, contribute to the Lorentz force acting on the charges inside volume V ,

$$\mathbf{f}_{\text{Lor}} = \rho \mathbf{E} + \rho \mathbf{v} \times \mathbf{B}, \quad (4.4)$$

where ρ is the density of charge and \mathbf{v} is the velocity of charges that contributes to current density $\rho \mathbf{v}$. The Lorentz force is zero for a neutral medium. The third term in Eq. (4.1), when integrated over volume V , is the measure of the rate of change of electromagnetic momentum inside the volume V ,

$$\mathbf{f}_m = \frac{\partial \mathbf{G}}{\partial t}. \quad (4.5)$$

This term is zero for slowly varying fields. The fourth term in Eq. (4.1) measures the flux of the electromagnetic field across the surface of the volume V and when integrated over a volume V , as a consequence of the Gauss law, measures the stress on the surface of the volume V due to the electromagnetic field. The force density due to this stress from the radiation is

$$\mathbf{f}_{\text{rad}} = -\nabla \cdot \mathbf{T}. \quad (4.6)$$

The fifth and the sixth term in Eq. (4.1) are the rate of transfer of electromagnetic energy to the dielectric and permeable material inside the volume V ,

$$\mathbf{f}_\varepsilon = -\frac{1}{2} E^2 \nabla \varepsilon, \quad (4.7a)$$

$$\mathbf{f}_\mu = -\frac{1}{2} H^2 \nabla \mu, \quad (4.7b)$$

respectively. Together, we have

$$\mathbf{f}_{\text{Lor}} + \mathbf{f}_m - \mathbf{f}_{\text{rad}} + \mathbf{f}_\varepsilon + \mathbf{f}_\mu = 0. \quad (4.8)$$

A. Stress tensor method

For a neutral dielectric medium, if we restrict to essentially static cases when the fields are varying slowly, three of the five terms in Eq. (4.8) can be neglected. In this case we have the relation

$$\mathbf{f}_{\text{rad}} = \mathbf{f}_\varepsilon + \mathbf{f}_\mu. \quad (4.9)$$

We choose the volume V in our discussion to be an infinitely thin film that encloses the surface of the dielectric medium. In the Boyer configuration of Fig. 1 this has been illustrated in Fig. 4. Eq. (4.9) is the statement of balance of forces. Integrating Eq. (4.6) over the volume V , and using Gauss's law, the left hand side of Eq. (4.9) gives the total radiation force on the left plate,

$$\mathbf{F}_{\text{rad}}(t) = - \oint_V d\mathbf{S} \cdot \mathbf{T}(\mathbf{r}, t). \quad (4.10)$$

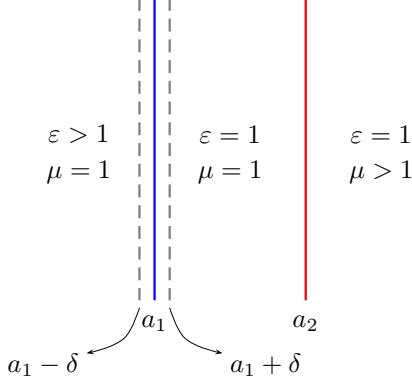


FIG. 4. Boyer configuration of parallel slabs with the illustration of the integration volume V . The integration volume V represents an infinitely thin film that encloses the surface of the dielectric slab at $z = a_1$. The surfaces of the film are at $z = a_1 - \delta$ and $z = a_1 + \delta$, and take the limit $\delta \rightarrow 0$.

The time averaged radiation force \mathbf{F}_{rad} is defined as the time average of $\mathbf{F}_{\text{rad}}(t)$, $\tau = 2T$,

$$\mathbf{F}_{\text{rad}} = \overline{\mathbf{F}_{\text{rad}}(t)} = \frac{1}{\tau} \int_{-T}^T dt \mathbf{F}_{\text{rad}}(t). \quad (4.11)$$

The stress tensor is a bilinear construction of the fields. For example, it involves the construction

$$\begin{aligned} \mathbf{E}(\mathbf{r}, t) \mathbf{D}(\mathbf{r}, t) &= \int_{-\infty}^{\infty} \frac{d\omega}{2\pi} \int_{-\infty}^{\infty} \frac{d\omega'}{2\pi} e^{-i(\omega' - \omega)t} \mathbf{E}(\mathbf{r}, \omega) \mathbf{D}(\mathbf{r}, \omega'), \end{aligned} \quad (4.12)$$

which uses the Fourier transformation

$$\mathbf{E}(\mathbf{r}, t) = \int_{-\infty}^{\infty} \frac{d\omega}{2\pi} e^{-i\omega t} \mathbf{E}(\mathbf{r}, \omega). \quad (4.13)$$

Time average of a bilinear construction satisfies the Plancherel theorem

$$\int_{-\infty}^{\infty} dt \mathbf{E}(\mathbf{r}, t) \mathbf{D}(\mathbf{r}, t) = \int_{-\infty}^{\infty} \frac{d\omega}{2\pi} \mathbf{E}(\mathbf{r}, \omega) \mathbf{D}(\mathbf{r}, \omega), \quad (4.14)$$

which implies

$$\int_{-\infty}^{\infty} dt \mathbf{T}(\mathbf{r}, t) = \int_{-\infty}^{\infty} \frac{d\omega}{2\pi} \mathbf{T}(\mathbf{r}, \omega). \quad (4.15)$$

Thus, we have, presuming $\tau = 2T \rightarrow \infty$,

$$\mathbf{F}_{\text{rad}} = -\frac{1}{\tau} \int_{-\infty}^{\infty} dt \oint_V d\mathbf{S} \cdot \mathbf{T}(\mathbf{r}, t) \quad (4.16a)$$

$$= -\frac{1}{\tau} \int_{-\infty}^{\infty} \frac{d\omega}{2\pi} \oint_V d\mathbf{S} \cdot \mathbf{T}(\mathbf{r}, \omega). \quad (4.16b)$$

The fluctuations in the quantum vacuum do not contribute to the mean value of the field and thus the field satisfies

$$\langle \mathbf{E} \rangle = 0, \quad (4.17)$$

but they contribute non-zero correlations in bilinear constructions of fields, and are contained in Eqs. (2.10). In particular, quantum vacuum fluctuations leads to non-zero contributions in the flux tensor. The radiation force arising from these contributions in the flux tensor, that are manifestations of the quantum vacuum, is a force given by

$$\mathbf{F} = -\frac{1}{2T} \int_{-\infty}^{\infty} \frac{d\omega}{2\pi} \oint_V d\mathbf{S} \cdot \langle \mathbf{T}(\mathbf{r}, \omega) \rangle. \quad (4.18)$$

We can write the force on the half-slab at $z = a_1$ to be

$$\frac{\mathbf{F} \cdot \hat{\mathbf{z}}}{A} = \frac{1}{i} \int_{-\infty}^{\infty} \frac{d\zeta}{2\pi} \int \frac{d^2 k_{\perp}}{(2\pi)^2} [T_{33}(a_1 + \delta) - T_{33}(a_1 - \delta)], \quad (4.19)$$

where, using Eq. (4.3),

$$\begin{aligned} T_{33}(a_1 - \delta) &= \frac{1}{2} [E_1^2 + E_2^2 - E_3^2] \Big|_{a_1 - \delta} \\ &\quad + \frac{1}{2} [H_1^2 + H_2^2 - H_3^2] \Big|_{a_1 - \delta} \end{aligned} \quad (4.20a)$$

$$\begin{aligned} &= \frac{\varepsilon}{2i} \left[\frac{\partial}{\varepsilon} \frac{\partial'}{\varepsilon} - \bar{\kappa}_{\varepsilon}^2 \right] g_{\text{①}}^H(a_1, a_1) \\ &\quad + \frac{1}{2i} [\partial \partial' - \kappa_{\varepsilon}^2] g_{\text{①}}^E(a_1, a_1) \end{aligned} \quad (4.20b)$$

and

$$\begin{aligned} T_{33}(a_1 + \delta) &= \frac{1}{2} [E_1^2 + E_2^2 - E_3^2] \Big|_{a_1 + \delta} \\ &\quad + \frac{1}{2} [H_1^2 + H_2^2 - H_3^2] \Big|_{a_1 + \delta} \end{aligned} \quad (4.21a)$$

$$= -\frac{\kappa^2}{i} [g_{\text{②}}^E(a_1, a_1) + g_{\text{②}}^H(a_1, a_1)]. \quad (4.21b)$$

The stress tensor $T_{33}(a_1 - \delta)$ is zero inside the perfect conductor. Thus, using Eq. (3.25), we obtain

$$P = \frac{\mathbf{F} \cdot \hat{\mathbf{z}}}{A} = \frac{1}{2\pi^2} \int_0^{\infty} \kappa^3 d\kappa \tanh \kappa a, \quad (4.22)$$

which can be rewritten in the form

$$P = \frac{1}{2\pi^2} \int_0^{\infty} \kappa^3 d\kappa \left[1 - \frac{2}{e^{2\kappa a} + 1} \right], \quad (4.23)$$

in which we have separated the divergent bulk contribution that does not have any information about the slabs. Subtracting the bulk contribution we have

$$P = -\frac{1}{\pi^2} \int_0^{\infty} \frac{\kappa^3 d\kappa}{e^{2\kappa a} + 1} = -\frac{7}{8} \frac{\pi^2}{240a^4}, \quad (4.24)$$

which is exactly the result obtained by Boyer. A negative force on the left plate corresponds to repulsion between the slabs.

B. Variation in dielectric method

The force on the dielectric slab can also be evaluated using the force density on the right hand side of Eq. (4.9), which is given by Eq. (4.7a) and is expressed in a more explicit form here,

$$\mathbf{f}_\varepsilon(\mathbf{r}, t) = -\frac{1}{2} \int_{-\infty}^{\infty} dt' \left[\nabla \varepsilon(\mathbf{r}, t - t') \right] \mathbf{E}(\mathbf{r}, t) \cdot \mathbf{E}(\mathbf{r}, t'). \quad (4.25)$$

In terms of frequency this takes the form

$$\begin{aligned} \mathbf{f}_\varepsilon(\mathbf{r}, t) &= -\frac{1}{2} \int_{-\infty}^{\infty} \frac{d\omega}{2\pi} \int_{-\infty}^{\infty} \frac{d\omega'}{2\pi} e^{-i(\omega - \omega')t} \\ &\times \left[\nabla \varepsilon(\mathbf{r}, \omega) \right] \mathbf{E}(\mathbf{r}, \omega')^* \cdot \mathbf{E}(\mathbf{r}, \omega). \end{aligned} \quad (4.26)$$

Time average of this force is calculated as, using $\tau = 2T \rightarrow \infty$,

$$\mathbf{F}_\varepsilon(\mathbf{r}) = \frac{1}{\tau} \int_{-\infty}^{\infty} dt \mathbf{f}_\varepsilon(\mathbf{r}, t) \quad (4.27a)$$

$$= -\frac{1}{2} \int_{-\infty}^{\infty} \frac{d\omega}{2\pi} \left[\nabla \varepsilon(\mathbf{r}, \omega) \right] \frac{1}{\tau} \mathbf{E}(\mathbf{r}, \omega')^* \cdot \mathbf{E}(\mathbf{r}, \omega). \quad (4.27b)$$

The force density, using Eq. (2.10a) in Eq. (4.27b), is defined as

$$\mathbf{F}(\mathbf{r}) = \langle \mathbf{F}_\varepsilon(\mathbf{r}) \rangle \quad (4.28a)$$

$$= -\frac{1}{2} \int_{-\infty}^{\infty} \frac{d\omega}{2\pi} \left[\nabla \varepsilon(\mathbf{r}, \omega) \right] \text{tr} \mathbf{\Gamma}(\mathbf{r}, \mathbf{r}; \omega), \quad (4.28b)$$

where trace tr is over the matrix index. The total force on a volume V is

$$\mathbf{F} = \int_V d^3r \mathbf{F}(\mathbf{r}) \quad (4.29a)$$

$$= -\frac{1}{2} \int_{-\infty}^{\infty} \frac{d\omega}{2\pi} \int_V d^3r \left[\nabla \varepsilon(\mathbf{r}, \omega) \right] \text{tr} \mathbf{\Gamma}(\mathbf{r}, \mathbf{r}; \omega). \quad (4.29b)$$

This expression, in contrast to the expression for the Casimir force Eq. (4.18), is another expression for the Casimir force of a fundamentally different origin. For planar configurations, using Eq. (3.1), and after switching to imaginary frequency, $\omega \rightarrow i\zeta$, the Casimir force per unit area on the slab at $z = a_1$ in Fig. 1 is

$$\begin{aligned} \frac{\mathbf{F} \cdot \hat{\mathbf{z}}}{A} &= -\frac{1}{2} \int_{-\infty}^{\infty} \frac{d\zeta}{2\pi} \int \frac{d^2 k_\perp}{(2\pi)^2} \int_{a_1 - \delta}^{a_1 + \delta} dz \\ &\times \left[\hat{\mathbf{z}} \cdot \nabla \varepsilon(\mathbf{r}, \omega) \right] \text{tr} \gamma(z, z; \mathbf{k}_\perp, \omega). \end{aligned} \quad (4.30)$$

For the Boyer configuration in Fig. 1 we have

$$\hat{\mathbf{z}} \cdot \nabla \varepsilon(\mathbf{r}, \omega) = -(\varepsilon - 1) \delta(z - a_1). \quad (4.31)$$

Assuming frequency independent dielectric function we have

$$\frac{\mathbf{F} \cdot \hat{\mathbf{z}}}{A} = \frac{(\varepsilon - 1)}{2} \int_{-\infty}^{\infty} \frac{d\zeta}{2\pi} \int \frac{d^2 k_\perp}{(2\pi)^2} \text{tr} \gamma(a_1, a_1; \mathbf{k}_\perp, \omega), \quad (4.32)$$

where

$$\begin{aligned} \text{tr} \gamma(a_1, a_1; \mathbf{k}_\perp, \omega) &= \frac{1}{\varepsilon(z)} \frac{\partial}{\partial z} \frac{1}{\varepsilon(z')} \frac{\partial}{\partial z'} g^H(z, z') \Big|_{z=a_1, z'=a_1} \\ &- \zeta^2 g^E(a_1, a_1) + \frac{k_\perp^2}{\varepsilon(z)\varepsilon(z')} g^H(a_1, a_1). \end{aligned} \quad (4.33)$$

The continuity conditions for the Green functions allows the evaluation of $g^E(a_1, a_1)$, $g^H(a_1, a_1)$, and $\partial \partial' g^H(a_1, a_1) / (\varepsilon \varepsilon')$, without caring about from which region in Fig. 3 the variables z and z' approach a_1 . This still leaves the regions from which z and z' approach a_1 in

$$\frac{k_\perp^2}{\varepsilon(z)\varepsilon(z')} \quad (4.34)$$

undetermined. Following the suggestion in Ref. [13] we will require z and z' to approach the interface at a_1 from opposite sides. This is necessary because otherwise the contribution to the Green dyadic from Eq. (3.3) will contribute spurious divergences. This is achieved by evaluating $\gamma(a_1, a_1; \mathbf{k}_\perp, \omega)$ in region ④ or in region ⑥ of Fig. 3. Thus,

$$\begin{aligned} \text{tr} \gamma_{\textcircled{4}}(a_1, a_1; \mathbf{k}_\perp, \omega) &= \frac{1}{\varepsilon} \partial \partial' g_{\textcircled{4}}^H(a_1, a_1) + \frac{k_\perp^2}{\varepsilon} g_{\textcircled{4}}^H(a_1, a_1) \\ &- \zeta^2 g_{\textcircled{4}}^E(a_1, a_1). \end{aligned} \quad (4.35)$$

The pressure in Eq. (4.32) involves the evaluation of

$$(\varepsilon - 1) \text{tr} \gamma_{\textcircled{4}}(a_1, a_1; \mathbf{k}_\perp, \omega), \quad (4.36)$$

which needs a little care when taking the perfect conductor limit. Observe that the electric Green function $g^E(a_1, a_1) = 0$. Thus, the term $\zeta^2(\varepsilon - 1)g^E(a_1, a_1)$ in the perfect conductor limit is ambiguous if we take the perfect conductor limit early in the calculation. To this end we define the parameter

$$s = 1 - r_\varepsilon, \quad (4.37)$$

which goes to zero in the perfect electric conductor limit. We note that

$$g_{\textcircled{4}}^E(a_1, a_1) = \frac{s}{2\kappa} \left[1 - s \frac{\bar{r}_\mu e^{-2\kappa a}}{\Delta^E} \right] \quad (4.38)$$

and

$$\zeta^2(\varepsilon - 1) = 4\kappa^2 \left(\frac{1}{s} - 1 \right) \frac{1}{s}, \quad (4.39)$$

which brings out the divergence structure and the related cancellations in the perfect conductor limit. Thus, the contribution from the TE-mode in Eq. (4.36) is

$$\text{TE:} \quad -\zeta^2(\varepsilon - 1)g_{\textcircled{4}}^E(a_1, a_1) = 2\kappa - \frac{2\kappa}{s} + 2\kappa \frac{r_\varepsilon \bar{r}_\mu}{\Delta^E} e^{-2\kappa a}. \quad (4.40)$$

The rest of the contributions in Eq. (4.36) is the TM-mode, which can be shown to be

$$\begin{aligned} \text{TM: } \frac{1}{\varepsilon} \partial \partial' g_{\text{TM}}^H(a_1, a_1) + \frac{k_{\perp}^2}{\varepsilon} g_{\text{TM}}^H(a_1, a_1) \\ = 2\kappa - \frac{2\kappa}{s} + 2\kappa \frac{\bar{r}_{\varepsilon} r_{\mu}}{\Delta^H} e^{-2\kappa a}. \end{aligned} \quad (4.41)$$

The evaluation of the contribution to the TM mode was assisted by the identities [14]

$$k_{\perp}^2 \pm \kappa \kappa_{\varepsilon} = -\frac{\bar{\kappa}_{\varepsilon} \mp \kappa}{\kappa_{\varepsilon} \mp \kappa} \zeta^2 \varepsilon. \quad (4.42)$$

Using the contribution from TE mode in Eqs. (4.40) and TM mode in Eq. (4.41) to evaluate Eq. (4.36), and using it in Eq. (4.32), and rewriting $2\kappa/s = \kappa_{\varepsilon} + \kappa$, the total pressure in Eq. (4.32) takes the form

$$\begin{aligned} \frac{\mathbf{F} \cdot \hat{\mathbf{z}}}{A} = \int_{-\infty}^{\infty} \frac{d\zeta}{2\pi} \int \frac{d^2 k_{\perp}}{(2\pi)^2} \\ \times \left[\kappa - \kappa_{\varepsilon} + \kappa \left(\frac{r_{\varepsilon} \bar{r}_{\mu}}{\Delta^E} + \frac{\bar{r}_{\varepsilon} r_{\mu}}{\Delta^H} \right) e^{-2\kappa a} \right], \end{aligned} \quad (4.43)$$

where Δ^E and Δ^H are given using Eqs. (3.13). The first term in Eq. (4.43) is the contribution from the empty space when the slabs are removed, which is divergent. The second term is the contribution due to the change in the single-body energy due to the variation in the dielectric medium, which is also divergent. The remaining term in the perfect conductor limit leads to

$$\frac{\mathbf{F} \cdot \hat{\mathbf{z}}}{A} = -\frac{1}{\pi^2} \int_0^{\infty} \frac{\kappa^3 d\kappa}{e^{2\kappa a} + 1} = -\frac{7}{8} \frac{\pi^2}{240a^4}. \quad (4.44)$$

Again, we reproduce the Boyer result.

C. Juxtaposition

In the Casimir (or Lifshitz) configuration of Fig. 2 when we require both slabs to have the same dielectric property, $\varepsilon > 1$, with no magnetic property, $\mu = 1$, we recall, for example in Ref. [13], the corresponding expression for the Casimir force to be

$$\begin{aligned} \frac{\mathbf{F}_{\text{Cas}} \cdot \hat{\mathbf{z}}}{A} = \int_{-\infty}^{\infty} \frac{d\zeta}{2\pi} \int \frac{d^2 k_{\perp}}{(2\pi)^2} \\ \times \left[\kappa - \kappa_{\varepsilon} + \kappa \left(\frac{r_{\varepsilon}^2}{\Delta_{\text{Cas}}^E} + \frac{\bar{r}_{\varepsilon}^2}{\Delta_{\text{Cas}}^H} \right) e^{-2\kappa a} \right], \end{aligned} \quad (4.45)$$

where

$$\Delta_{\text{Cas}}^E = 1 - r_{\varepsilon}^2 e^{-2\kappa a}, \quad (4.46a)$$

$$\Delta_{\text{Cas}}^H = 1 - \bar{r}_{\varepsilon}^2 e^{-2\kappa a}. \quad (4.46b)$$

In the perfect conductor limit the expression in Eq. (4.45) takes the form

$$\frac{\mathbf{F}_{\text{Cas}} \cdot \hat{\mathbf{z}}}{A} = \frac{1}{\pi^2} \int_0^{\infty} \frac{\kappa^3 d\kappa}{e^{2\kappa a} - 1} = \frac{\pi^2}{240a^4}, \quad (4.47)$$

which is the attractive Casimir pressure on the left perfect conducting slab.

The display of Eq. (4.43), that leads to the Boyer force, and Eq. (4.45), that leads to the Casimir force, brings out the close similarity in the two expressions, and reveals the fine differences between them. We observe that the difference in the reflection coefficients of the second slab in the Boyer and Casimir configurations in Figs. 1 and 2 is the source of the dissimilarity in the two expressions. We note that the relative sign difference between the Boyer and the Casimir configuration arises because in the perfect electric conducting limit ($\varepsilon \rightarrow \infty$) and perfect magnetic conducting limit ($\mu \rightarrow \infty$) we obtain a relative sign difference,

$$r_{\varepsilon} \bar{r}_{\mu} \rightarrow -1, \quad \text{and} \quad \bar{r}_{\varepsilon} r_{\mu} \rightarrow -1, \quad (4.48)$$

versus

$$r_{\varepsilon}^2 \rightarrow 1, \quad \text{and} \quad \bar{r}_{\varepsilon}^2 \rightarrow 1. \quad (4.49)$$

Thus, in perfect conducting limits, after dropping the first two divergent terms in Eqs. (4.43) and (4.45), that removes the bulk and single-body contributions, the expression for the pressure on the left slab is given by the third term in Eqs. (4.43) and (4.45), which differ by an overall sign, in addition to the difference in sign in their denominators. This is the difference in sign (direction) between the pressures on the left slab in the Boyer and Casimir configuration. We also note that, in the perfect conducting limits, Δ^E and Δ^H for the Boyer configuration go to $1 + e^{-2\kappa a}$, while the corresponding factors Δ_{Cas}^E and Δ_{Cas}^H in the Casimir configuration go to $1 - e^{-2\kappa a}$. These renders to the difference in sign in the denominators of Eqs. (4.44) and (4.47), and leads to the classic relative factor of

$$\frac{7}{8} = \frac{\int_0^{\infty} \frac{\kappa^3 d\kappa}{e^{2\kappa a} + 1}}{\int_0^{\infty} \frac{\kappa^3 d\kappa}{e^{2\kappa a} - 1}} \quad (4.50)$$

in Eq. (4.44).

The Boyer configuration and the Casimir configuration of Figs. 1 and 2 can, both, independently, be interpreted to form a cavity, which are by construction different in their constituent boundaries. We shall call them the Boyer cavity and the Casimir cavity. If a monochromatic electromagnetic wave completes one closed loop in a Casimir cavity, involving a reflection off the right dielectric slab and then a reflection off the left dielectric slab, it is effectively unchanged, because $r_{\varepsilon}^2 = 1$. On the other hand, if a monochromatic electromagnetic wave completes a closed loop in a Boyer cavity, it develops a phase difference of π because $r_{\varepsilon} \bar{r}_{\mu} = -1$. Further, after completing two closed loops in a Boyer cavity the wave returns back to its original state. In this sense, the Boyer cavity is topologically different from a Casimir cavity.

In the multiple scattering formalism, the Casimir force and the Boyer force can be interpreted as the sum of all

possible scattering inside the respective cavities. That is, the integrals in Eqs. (4.44) and (4.47), respectively, are interpreted as the sum of all possible permutations and combinations of scattering possible in the respective cavities. This can be more explicitly illustrated by expanding the integrand of Eqs. (4.44) and (4.47), as a binomial expansion in $e^{-2\kappa a}$. This assemblage of all possible permutations and combinations of scattering inside a cavity gives the cavity itself a statistical identity. In other words, the spectral distribution of scattering inside a Casimir cavity is described by Bose-Einstein distribution, while the spectral distribution of scattering inside a Boyer cavity is described by Fermi-Dirac distribution. Thus, in conclusion, the source for the difference in the Casimir force and the Boyer force lies in the fact that the respective cavities have fundamentally different statistics describing the scattering inside the respective cavities.

The Boyer configuration and the Casimir configuration in Figs. 1 and 2 are special cases of more general boundary conditions that has been studied for two magneto-electric δ -function plates in Ref. [15]. Similar general boundary conditions for a scalar field has been extensively studied in Ref. [16]. This, then, suggests a class of statistics associated with the distribution of scatterings inside such general configurations. However, these characteristics are dependent on the parameters describing the material. The special extreme limits of Boyer and Casimir configuration has the nice feature that it has no dependence on the particular material properties.

V. FINITE COUPLING USING STRESS TENSOR METHOD

The perfect coupling limit in Sec. III C and Sec. IV is an extreme limit, and it is instructive to consider the finite coupling case for real materials. We need to evaluate the pressure along the z -direction given in (4.19) using the scalar electric and magnetic Green's functions for the finite value of permittivity and permeability in Eqs. (4.20b) and (4.21b). We obtain

$$T_{33}(a_1 - \delta) = -\frac{\kappa_\varepsilon}{i}, \quad (5.1)$$

which is just the contribution coming from the single-body bulk terms in the Green function. While

$$T_{33}(a_1 + \delta) = -\frac{\kappa}{i} - \frac{\kappa}{i} \left(\frac{r_\varepsilon \bar{r}_\mu}{\Delta^E} + \frac{\bar{r}_\varepsilon r_\mu}{\Delta^H} \right) e^{-2\kappa a}. \quad (5.2)$$

Dropping the bulk contributions in $T_{33}(a_1 - \delta)$ and $T_{33}(a_1 + \delta)$ in Eqs. (5.1) and (5.2) we find

$$P_\varepsilon = \int_{-\infty}^{\infty} \frac{d\zeta}{2\pi} \int \frac{d^2 k_\perp}{(2\pi)^2} \kappa \left(\frac{r_\varepsilon \bar{r}_\mu}{\Delta^E} + \frac{\bar{r}_\varepsilon r_\mu}{\Delta^H} \right) e^{-2\kappa a}, \quad (5.3)$$

which is identical to the what we obtained in Eq. (4.43), if the dropped terms were reintroduced. We can write

Eq. (5.3) in spherical polar co-ordinate system after defining $k_\perp = \kappa \sin \theta$ and $\zeta = \kappa \cos \theta$, then it is straightforward to carry out the κ integration, to obtain

$$P_\varepsilon = \frac{3}{16\pi^2 a^4} \int_0^1 dt [\text{Li}_4(r_\varepsilon \bar{r}_\mu) + \text{Li}_4(\bar{r}_\varepsilon r_\mu)], \quad (5.4)$$

where $\text{Li}_4(x)$ is the polylogarithm function and

$$r_\varepsilon(t) = \frac{\sqrt{1 + (\varepsilon - 1)t^2} - 1}{\sqrt{1 + (\varepsilon - 1)t^2} + 1}, \quad (5.5a)$$

$$r_\mu(t) = \frac{\sqrt{1 + (\mu - 1)t^2} - 1}{\sqrt{1 + (\mu - 1)t^2} + 1}, \quad (5.5b)$$

and

$$\bar{r}_\varepsilon(t) = \frac{\sqrt{1 + (\varepsilon - 1)t^2} - \varepsilon}{\sqrt{1 + (\varepsilon - 1)t^2} + \varepsilon}, \quad (5.6a)$$

$$\bar{r}_\mu(t) = \frac{\sqrt{1 + (\mu - 1)t^2} - \mu}{\sqrt{1 + (\mu - 1)t^2} + \mu}. \quad (5.6b)$$

It is not a priori obvious whether this pressure is attractive or repulsive on the left boundary. Even for the simple non-dispersive case it is not easy to do the remaining integration analytically. The plot of the integrand from 0 to 1 is always negative, implying that the pressure on the left boundary is still repulsive. We can carry out the integration numerically and observe that the ratio of the pressure on left wall for the real material to the Boyer's pressure is always positive and approaches Boyer's result for very large values of permittivity and permeability.

To make our analysis include dispersion, we resolve to a simple model for the permeability as described in Eq. (1.11) in which we breakup the frequency integration in (5.3) into two parts. We assume μ to be constant up to a critical frequency $\zeta_c = -i\omega_c$, thereafter we set $\mu = 1$. Clearly, we will not get any contribution for the higher frequencies beyond ζ_c for our system as there is no interface on the right when $\mu = 1$.

In Fig. 5, we plot the pressure P_ε normalized to the Boyer value for the perfectly conducting case P_∞ as a function of the dimensionless product $\zeta_c a$ in Eq. (1.11) for different values of permittivity and permeability. For reference, at $a = 1 \mu\text{m}$ the cutoff frequency is $\omega_c = c/a = 3 \times 10^{14}$ Hz. The positive values for P_ε/P_∞ implies that the pressure between a real electric and magnetic media is still repulsive. For very high values of respective permittivity and permeability of two media, the Casimir pressure approaches Boyer's result as expected, while for more realistic values it remains less than Boyer's result. Realistic frequency responses in magnetic materials do not go beyond 1 MHz, which corresponds to $\zeta_c a \sim 10^{-8}$ for $a = 1 \mu\text{m}$, for which the pressure is immeasurably small. This connects with the fact that the Boyer repulsion has never been experimentally measured.

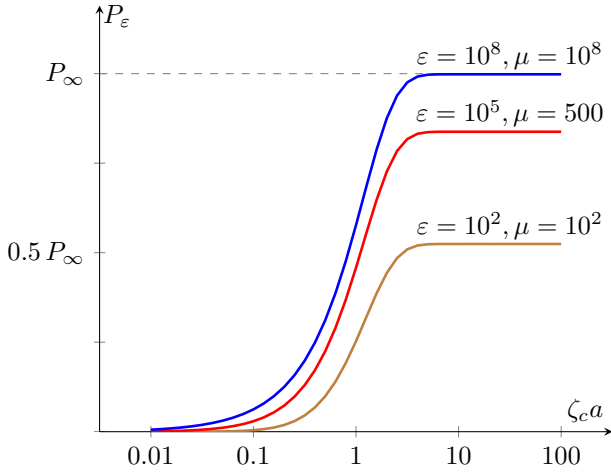


FIG. 5. The Casimir pressure on the left interface of a material medium with electrical permittivity ε interacting with a material medium of magnetic permeability μ with cutoff frequency ζ_c in Eq. (1.11) plotted as a function of $(\zeta_c a)$. Here P_∞ is the Boyer result for the perfectly electrically conducting and perfectly magnetically conducting half-spaces. Realistic frequency responses in magnetic materials do not go beyond 1 MHz, which corresponds to $\zeta_c a \sim 10^{-8}$ for $a = 1 \mu\text{m}$, for which the pressure is immeasurably small.

VI. STATISTICAL MECHANICAL CONSIDERATIONS

In this section we try to give an alternative explanation of the Boyer problem by drawing quantum statistical mechanics into consideration.

Let the two media (half-spaces), separated by a gap a , be general dielectrics endowed with arbitrary constant values of ε and μ . We introduce a model where the media are represented by harmonic oscillators 1 and 2, interacting with each other via a third oscillator 3. The last oscillator represents the electromagnetic field. In the generalized version of the model, the third oscillator represents an assembly of oscillators. An advantage of this model is that it provides a mechanical analogue to the conventional TE and TM modes in electromagnetism. Among these, the TM modes are the easiest ones to visualize, among else things because the induced interaction increases when the temperature T increases, so as to reach the classical limit for high T . By contrast, in the TE case the force goes to zero in the classical case because the zero Matsubara frequency will not contribute. And, as we will show, this harmonic oscillator model is able to shed some further light on the Boyer problem also. We have actually introduced the model in earlier works, in connection with the Casimir effect, [17–19], although the model does not seem to be well known.

Let us sketch some essentials of the formalism. As is known, the classical partition function Z of a harmonic oscillator is $Z = 1/(\hbar\beta\omega_i)$, with $\beta = 1/(k_B T)$, where ω_i here is the eigen frequency of an oscillator. It means that

the free energy is

$$F = -\frac{1}{\beta} \ln Z \sim \ln \omega_i. \quad (6.1)$$

If three noninteracting oscillators the inverse partition function is thus proportional to \sqrt{Q} , where

$$Q = a_1 a_2 a_3, \quad a_i = \omega_i^2 \quad (i = 1, 2, 3). \quad (6.2)$$

When going over to quantum statistical mechanics (path integral method [20, 21]), the classical system is imagined to be divided into a set of classical harmonic oscillator systems. It implies the substitutions

$$Q = A_1 A_2 A_3, \quad A_i = a_i + \zeta^2 = \omega_i^2 + \zeta^2 \quad (6.3)$$

where now $\zeta = i\omega$ is the Matsubara frequency.

We assume that oscillators 1 and 2 interact via oscillator 3, and assume for simplicity that all oscillators are one-dimensional. Taking the interaction to be bilinear, thus expressible in the form $c x_i x_j$ with c a coupling constant, we obtain the following determinant

$$Q = \begin{vmatrix} A_1 & 0 & c \\ 0 & A_2 & c \\ c & c & A_3 \end{vmatrix} = A_1 A_2 A_3 (1 - D_1)(1 - D_2) \times \left[1 - \frac{D_1 D_2}{(1 - D_1)(1 - D_2)} \right], \quad (6.4a)$$

where

$$D_j = \frac{c^2}{A_j A_3} \quad (j = 1, 2). \quad (6.5)$$

Here the first term $A_1 A_2 A_3$ refers to the noninteracting oscillators. The terms $A_j(1 - D_j)$ ($j = 1, 2$) are the separate interactions between 1-3 and 2-3, while the last term is the Casimir energy. If $Q > 0$, the Casimir energy is negative, corresponding to an attractive force.

This is the straightforward part of the analysis, and corresponds to the electromagnetic TM mode. The TE mode is more intricate, as it corresponds to oscillator 3 interacting with the *momenta* of oscillators 1 and 2. The interaction replaces the term $p_j^2/2m_j$ with $(\mathbf{p}_j - e\mathbf{A})^2/2m_j$, where \mathbf{p}_j is the canonical momentum and \mathbf{A} the vector potential. In the oscillator model the analogous energy takes the form

$$\frac{1}{2} m_j a_j \left(p_j - \frac{c}{a_j} x_3 \right)^2 \quad (6.6)$$

Now again c is the coupling parameter and x_3 corresponds to A_3 .

The important outcome of this is that the A_3 in the determinant Q is changed,

$$A_3 \rightarrow A_3 + \frac{c^2}{a_1} + \frac{c^2}{a_2}. \quad (6.7)$$

This means that Q can be written as

$$Q = \begin{vmatrix} A_1 & 0 & c \\ 0 & A_2 & c \\ cq_1 & cq_2 & A_3 \end{vmatrix} = \begin{vmatrix} A_1 & 0 & \frac{\zeta c}{\sqrt{a_1}} \\ 0 & A_2 & \frac{\zeta c}{\sqrt{a_2}} \\ -\frac{\zeta c}{\sqrt{a_1}} & -\frac{\zeta c}{\sqrt{a_2}} & A_3 \end{vmatrix}, \quad (6.8)$$

using the property of determinants in the second equality, where

$$q_j = 1 - \frac{A_j}{a_j} = -\frac{\zeta^2}{a_j}, \quad (j = 1, 2). \quad (6.9)$$

The determinant Q can still be expressed as in Eq. (6.4a), but now with

$$D_j = -\frac{\zeta^2 c^2}{a_j A_j A_3} < 0. \quad (6.10)$$

The induced force is still attractive since $D_1 D_2 > 0$, although both factors are negative.

Proceed now to the third and final step. Assume for definiteness that only oscillator $j = 2$ has the form (6.6). Then A_3 changes to

$$A_3 \rightarrow A_3 + \frac{c^2}{a_2}, \quad (6.11)$$

and the determinant (6.8) changes to

$$Q = \begin{vmatrix} A_1 & 0 & c \\ 0 & A_2 & \frac{\zeta c}{\sqrt{a_2}} \\ c & -\frac{\zeta c}{\sqrt{a_2}} & A_3 \end{vmatrix}. \quad (6.12)$$

This implies that

$$D_1 = \frac{c^2}{A_1 A_3} > 0 \quad \text{and} \quad D_2 = -\frac{\zeta^2 c^2}{a_j A_j A_3} < 0, \quad (6.13)$$

so that $D_1 D_2 < 0$ and the induced force becomes repulsive.

Looking back, we are now able to summarize what were the characteristic properties of the harmonic oscillator model making the transition from an attractive to a repulsive force possible:

1. The generalization $a_i \rightarrow A_i$ in Eq. (6.3), meaning incorporation of the discrete Matsubara frequencies ζ ;
2. the modification of A_3 in Eq. (6.7), corresponding to the transition from the TM to the TE mode. In turn, this is related to the oscillator 3 interacting with oscillators 1 and 2 via canonical momenta p_j , instead of via positions x_i (interaction energy $cx_i x_j$) as was characteristic for the TM mode.

When seen in this way, the basic reason for the Boyer problem is linked to quantum mechanics. This is a satisfactory conclusion, since otherwise, in classical electrodynamics, the sign reversal of E^2 in the force expression $-\frac{1}{2}E^2 \nabla \varepsilon$ as noted above, would be quite non-understandable.

ACKNOWLEDGMENTS

We acknowledge support from the Research Council of Norway (Project No. 250346).

-
- [1] K. A. Milton, *The Casimir Effect: Physical Manifestations of Zero-Point Energy* (World Scientific, River Edge, USA, 2001).
 - [2] M. Bordag, G. L. Klimchitskaya, U. Mohideen, and V. M. Mostepanenko, *Advances in the Casimir Effect*, Int. Ser. Monogr. Phys., Vol. 145 (Oxford University Press, New York, 2009).
 - [3] D. Dalvit, P. Milonni, D. Roberts, and F. da Rosa, eds., *Casimir Physics*, Lecture Notes in Physics, Vol. 834 (Springer, Berlin, 2011).
 - [4] T. H. Boyer, “Van der Waals forces and zero-point energy for dielectric and permeable materials,” *Phys. Rev. A* **9**, 2078 (1974).
 - [5] A. Ashkin and J. M. Dziedzic, “Radiation pressure on a free liquid surface,” *Phys. Rev. Lett.* **30**, 139 (1973).
 - [6] N. G. C. Astrath, L. C. Malacarne, M. L. Baesso, G. V. B. Lukasiewicz, and S. E. Bialkowski, “Unravelling the effects of radiation forces in water,” *Nature Comm.* **5**, 4363 (2014).
 - [7] I. Brevik, “Minkowski momentum resulting from a vacuum-medium mapping procedure, and a brief review of Minkowski momentum experiments,” *Ann. Phys. (N.Y.)* **377**, 10 (2017).
 - [8] A. Kundu, R. Rani, and K. S. Hazra, “Graphene oxide demonstrates experimental confirmation of Abraham pressure on solid surface,” *Scientific Rep.* **7**, 42538 (2017).
 - [9] L. D. Landau and E. M. Lifshitz, *Electrodynamics of Continuous Media*, 2nd ed., Course of Theoretical Physics, Vol. 8 (Pergamon, Amsterdam, 1984) sec. 79.
 - [10] “Tables of Physical & Chemical Constants,” (Kaye & Laby Online, The National Physical Laboratory, 2005) Chap. 2.6.6 Magnetic properties of materials, version 1.0.
 - [11] P. Parashar, K. A. Milton, K. V. Shajesh, and M. Schaden, “Electromagnetic semitransparent δ -function plate: Casimir interaction energy between parallel infinitesimally thin plates,” *Phys. Rev. D* **86**, 085021 (2012).
 - [12] P. Parashar, K. A. Milton, Y. Li, H. Day, X. Guo, S. A. Fulling, and I. Cavero-Peláez, “Quantum electromag-

- netic stress tensor in an inhomogeneous medium,” Phys. Rev. D **97**, 125009 (2018), [arXiv:1804.04045 \[hep-th\]](#).
- [13] J Schwinger, L. L. DeRaad, and K. A. Milton, “Casimir effect in dielectrics,” Ann. Phys. **115**, 1 (1978).
- [14] P. Parashar, *Geometrical investigations of the Casimir effect: Thickness and corrugations dependencies*, Ph.D. thesis, The University of Oklahoma, Norman (2011).
- [15] K. A. Milton, P. Parashar, M. Schaden, and K. V. Shajesh, “Casimir interaction energies for magneto-electric δ -function plates,” *Proceedings, Mathematical Structure in Quantum Systems and applications (MSQS2012): Benasque, Spain, July 8-14, 2012*, Nuovo Cim. C **36**, 193 (2013), [arXiv:1302.0313 \[hep-th\]](#).
- [16] M. Asorey and J. M. Munoz-Castaneda, “Attractive and repulsive Casimir vacuum energy with general boundary conditions,” Nucl. Phys. B **874**, 852 (2013), [arXiv:1306.4370 \[hep-th\]](#).
- [17] J. S. Høye, I. Brevik, J. B. Aarseth, and K. A. Milton, “Does the transverse electric zero mode contribute to the Casimir effect for a metal?” Phys. Rev. E **67**, 056116 (2003).
- [18] J. S. Høye, I. Brevik, and K. A. Milton, “Presence of negative entropies in Casimir interactions,” Phys. Rev. A **94**, 032113 (2016).
- [19] J. S. Høye and I. Brevik, “Repulsive Casimir force,” Phys. Rev. A (2018), accepted for publication, [arXiv:1805.06224 \[quant-ph\]](#).
- [20] J. S. Høye and G. Stell, “Theory of the refractive index of fluids,” J. Chem. Phys. **77**, 5173 (1982).
- [21] I. Brevik and J. S. J.S. Høye, “Van der Waals force derived from a quantum statistical mechanical path integral method,” Physica A **153**, 420 (1988).